Drug Development and Industrial Pharmacy, 2009; 35(10): 1167–1179

informa
healthcare

ORIGINAL ARTICLE

Hollow spherical nanoparticulate aggregates as potential ultrasound contrast agent: shell thickness characterization

Kunn Hadinoto and Wean Sin Cheow

School of Chemical and Biomedical Engineering, Nanyang Technological University, Singapore

Abstract

Objective: The objective of this work is to manufacture hollow spherical nanoparticulate aggregates for use as an ultrasound contrast agent by means of spray drying of nanoparticulate suspension at a fast drying rate. *Methodology*: Biocompatible PMMA-MeOPEGMA and silica nanoparticles are used as the model nanoparticles. The impacts of changing the nanoparticle concentration, pH, and spray drying operating condition on the size and shell thickness-to-particle radius (*S/R*) ratio, which governs the shell mechanical stability, are investigated. *Results and conclusion*: The results indicate that the hollow microspheres size varies between 2 and 10 μm having *S/R* ratio between 2% and 4%, where the smaller size particles exhibit a higher *S/R* ratio. The resultant *S/R* ratio is found to be more influenced by process parameters acting at the nanoparticle scale (e.g., suspension pH) than by the spray drying operating condition.

Key words: *Hollow aggregates; nanoparticles; shell thickness; spray drying; ultrasound contrast agent*

Introduction

Medical ultrasonography is one of the most widely performed noninvasive medical diagnostic tests, whose principle is based on detecting and quantifying the shift in the Doppler frequency of the backscattered acoustic signal from the organ tissue being imaged. The conventional ultrasonography, however, lacks the capability to image microvascular blood flows in the tissue of an organ or a tumor because of the similar echogenicity levels of the backscattered acoustic signals from the organ tissue and the blood capillary. For that reason, ultrasound contrast agents, in the form of hollow microspheres that are delivered intravenously, are employed in tissue perfusion imaging to enhance the signal amplitude of the blood flow relative to that of the tissue[1]. The ultrasound contrast enhancement is attributed to 1) a strong acoustic signal generated by the radial oscillation of the compressible gas inside the hollow microspheres under an acoustic field and 2) the density difference between the gas-filled microspheres and the surrounding tissue[2].

Current ultrasound contrast agents typically comprise a gas core that is encapsulated within a solid shell of polymer, lipid, or surfactant materials. The contrast agent effectiveness is governed by (1) the particle size, (2) the aqueous diffusivity and solubility of the encapsulated gas, and (3) the structural stability of the shell during ultrasonic excitation[3]. First, a large particle size is preferred as it generates a strong ultrasound signal; however, the largest particle size must be smaller than the blood capillary size (i.e., <10 μm). Second, high-molecular-weight gases with low diffusion coefficients and low aqueous solubility (e.g., perfluorocarbons) are often used in place of air to minimize the gas outward diffusion hence extending the contrast agent lifespan. Third, a complete shell fragmentation or a gas outward diffusion through a shell defect, which occurs at a high acoustic power, can be avoided by using a polymeric shell that exhibits a higher structural stability than that of the lipid or surfactant-based shells[4].

The structural stability of a shell in the classical mechanics theory is governed by the ratio of the shell thickness to the particle radius (*S/R*), where *S* is the

Address for correspondence: Professor Kunn Hadinoto, Nanyang Technological University, School of Chemical and Biomedical Engineering, Singapore 637459, Singapore. Tel: +65 6514 8381. E-mail: kunnong@ntu.edu.sg

(Received 18 Nov 2008; accepted 13 Feb 2009)

ISSN 0363-9045 print/ISSN 1520-5762 online © Informa UK, Ltd.
DOI: 10.1080/03639040902824845

shell thickness and R is the hollow particle radius[5] . Hollow particles with a high S/R ratio exhibit a high stability in which the shell is less prone to fragmentation[6]. For such particles, a higher ultrasound frequency (i.e., higher energy) was needed to destabilize the shell[7].

The hollow microspheres for ultrasound contrast agents are typically manufactured by a two-step process, which consists of 1) an emulsification step in which a liquid/solid core of a volatile foaming agent (e.g., ammonium bicarbonate) is encapsulated by a polymeric shell and 2) a drying step in which the liquid/solid core is removed by either freeze or spray drying to create hollow microspheres in a dry powder form[8–11]. All these works meticulously investigated the effects of the process parameters on the size of the hollow microspheres, which dictates the echogenicity level. Unfortunately, a less emphasis was placed on the shell thickness though it is equally important as it governs the shell stability. Importantly, the drawback of this manufacturing technique is that the hollow microspheres morphology (i.e., size and shell thickness) is highly influenced by both the encapsulation and the drying processes. Consequently, an excessive number of process parameters must be considered and subsequently optimized during the process design stage, which reduces its scale-up feasibility and predictability.

For that reason, Pisani et al.[12] recently developed a simple one-step emulsification technique to encapsulate liquid perfluorocarbons within a polymeric shell producing microcapsules, whose S/R ratio was controlled by modifying the polymer-to-perfluorocarbons ratio before the emulsification step. Schmidt and Roessling[13] developed a novel technique to manufacture nanocomposite hollow microspheres by homogenization of surfactant-coated polymeric nanoparticles using micron-size bubbles as a template. In this work, another powerful yet simple technique to manufacture hollow microspheres, by means of spray drying of an aqueous suspension of polymeric nanoparticles, is developed (Figure 1). The spray-dried particles exhibit a hollow structure, whose shells are composed of nanoparticulate aggregates that are held together by physical attractive forces (i.e., capillary and van der Waals forces). Importantly, this technique is significantly less time-intensive compared with the other techniques mentioned above, which is attributed to the simplicity of the spray-drying process.

This technique was first developed by the authors to manufacture micron-size carrier particles of nanoparticulate drug for pulmonary drug delivery using a dry powder inhaler[14]. The main objective of Hadinoto et al. was to manufacture large and hollow spherical nanoparticulate aggregates (≈15–20 μm) designed to improve the aerosolization efficiency and the lung deposition of the inhaled particles. A less emphasis was placed on the structural stability of the shell (i.e., S/R ratio), because the particles were not anticipated to be exposed to high-intensity destabilizing forces in a dry powder inhaler. The shell stability and lifespan of the hollow nanoparticulate aggregates become significantly more important if they are to be used as an ultrasound contrast agent[15]. For that reason, this work aims to investigate the effects of the experimental condition on the resultant S/R ratio.

To identify the important process parameters, the detailed physical mechanism behind the hollow nanoparticulate aggregate formation is illustrated in Figure 2. Evaporation of the liquid from the droplet surface causes the nanoparticles at the receding liquid–vapor interface being exposed to the vapor phase. As the surface energy of a solid–vapor interface is greater than that of a liquid–vapor interface, the exposed nanoparticles migrate

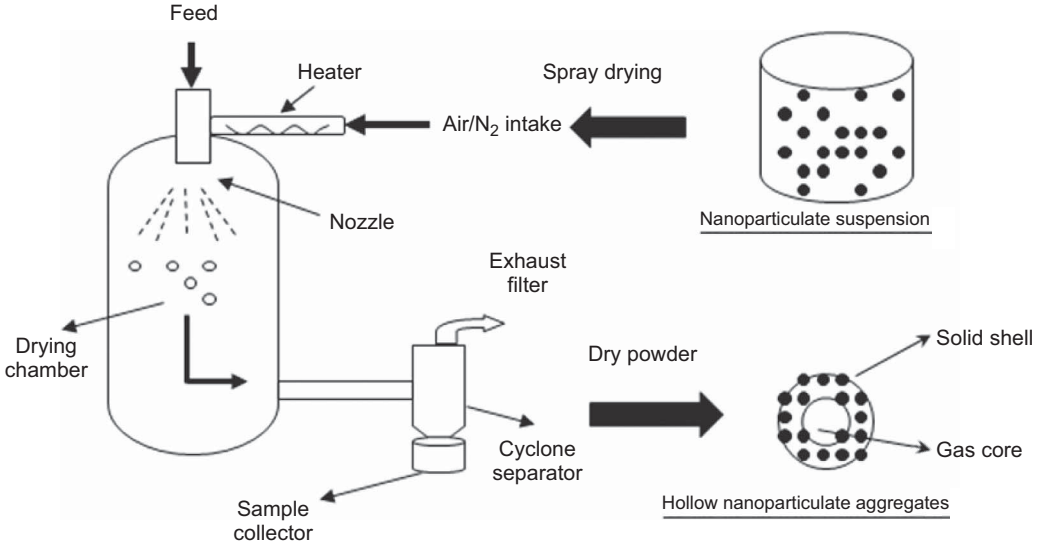

Figure 1. Hollow microspheres produced by spray drying of nanoparticulate suspension.

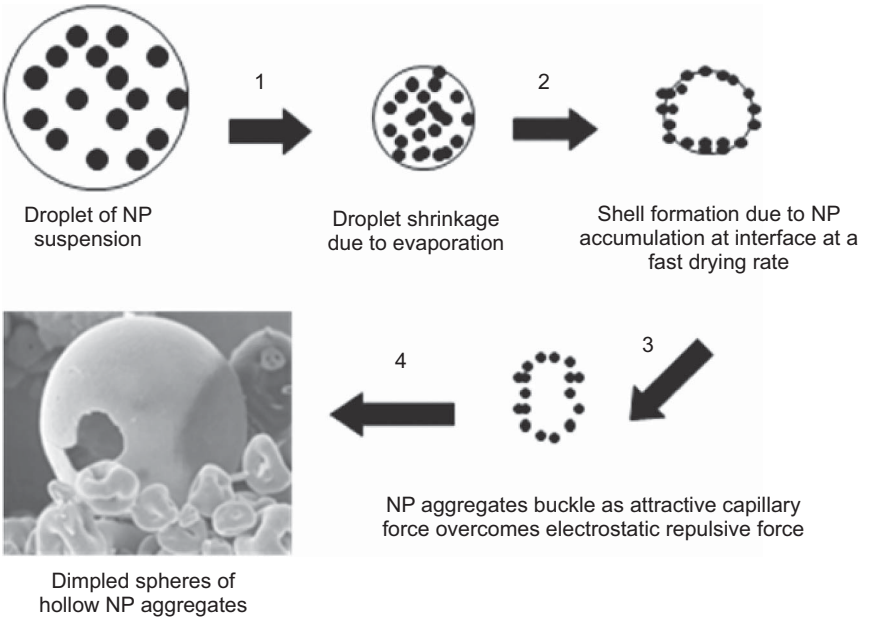

Figure 2. Physical mechanisms behind the hollow nanoparticulate (NP) aggregates formation.

toward the droplet center to minimize their surface energy. To produce the hollow nanoparticulate aggregates, a fast convective drying rate, where the time for the liquid evaporation is shorter than the time for the nanoparticles to diffuse back toward the droplet center, is required. A fast convective drying rate is obtained when the local Peclet number (*Pe*) is significantly larger than unity. *Pe* defined in Equation (1) signifies the relative importance of the time scale of the nanoparticle diffusion (R^2/D_S) with respect to that of the convective drying rate (τ_D).

$$Pe = \frac{R^2}{\tau_D D_S}, \tag{1}$$

where r, τ_D, and D_S are the droplet radius, drying time, and nanoparticle diffusion coefficient, respectively.

For $Pe >> 1$, the nanoparticle diffusion rate toward the droplet center is slower than the convective drying rate leading to the shell formation. As the shell begins to form, the capillary force generated by the meniscus formed in the gap between the nanoparticles drives the nanoparticles closer forming the nanoparticulate aggregates. This attractive capillary force, however, is resisted by the repulsive electrostatic force acting as a stabilizer against the aggregation process. The competing interaction between these two forces leads to a shell buckling phenomenon that influences the resultant shell thickness[16]. This phenomenon is manifested in the formation of dimpled hollow microspheres (Figure 2). Importantly, the shell-buckling process is influenced by the nanoparticle concentration, the droplet evaporation rate, and the nanoparticle surface forces.

The specific aim of this work is to examine the ability of the present technique to manufacture hollow nanoparticulate aggregates of varying *S/R* ratio. For this purpose, the effects of the following process parameters: 1) the nanoparticulate suspension concentration, 2) its pH, and 3) the spray-drying operating condition that governs the droplet evaporation rate are investigated. Biocompatible polymeric nanoparticles of poly(methyl-methacrylate) conjugated with methoxy(polyethylene-glycol)methacrylate (PMMA-MeOPEGMA) are used as the model nanoparticle to be employed as an ultrasound contrast agent.

Acrylic-based polymer, such as PMMA-MeOPEGMA, is well known to exhibit a high mechanical strength suited for the spray-drying process in which a high shear force is exerted by the drying gas on the sprayed droplets containing the polymeric nanoparticles. Furthermore, the high mechanical strength of the polymeric nanoparticles is expected to make the hollow nanoparticulate aggregates exhibit a high shell stability that renders them an ideal ultrasound contrast agent. The spray-drying experiment is also conducted using commercially available silica, poly(lactide-co-glycolide) (PLGA), and polystyrene nanoparticles to examine the robustness of the present technique in producing the hollow nanoparticulate aggregates from nanoparticles of different chemical nature.

Methodology

Materials

The monomers for the synthesis of the polymeric nanoparticles, that is, methyl methacrylate (MMA), butyl

acrylate (BA), acrylic acid (AA), methoxy(polyethylene glycol)methacrylate (MeOPEGMA, Mw = 2000), and the initiator 4,4-Azobis(4-cyanovaleric acid) (carboxy ADIB, purity ≥75%) are purchased from Sigma-Aldrich (St. Louis, MO, USA), except for the MeOPEGMA, which is kindly supplied by Cognis Performance Chemicals (Southampton, UK). Aqueous suspension of colloidal silica Ludox TM-40 [pH = 9.0; 40% (w/v); 20 ± 10 nm], ethyl acetate, ethanol, Trizma base, hydrochloric acid, and potassium hydroxide are also purchased from Sigma-Aldrich. PLGA resomer is purchased from Boehringer Ingelheim (Ingelheim, Germany). Aqueous suspension of polystyrene nanoparticles [pH = 7.0; 4% (w/v); 100 ± 6 nm] is purchased from Interfacial Dynamics (Portland, OR, USA).

Preparation of polymeric nanoparticles

The PMMA-MeOPEGMA polymer is prepared by a solution tetrapolymerization of MeOPEGMA, MMA, BA, and AA in the proportions 15, 69, 11, and 5 (% w/w), respectively. Ethyl acetate and ethanol are used as the solvents. The polymer is converted into nanoparticles by the solvent replacement technique. The nanoparticles exhibit steric colloidal stability arising from the MeOPEGMA component. Briefly, 0.15 g carboxy ADIB is dissolved in 15 mL ethanol and then 55 mL ethyl acetate is added. The solution is refluxed for 45 minutes at 90°C in a water-cooled reflux condenser. For the 1st feed solution, 0.13 g carboxy ADIB and 12.7 g MeOPEGMA are dissolved in 6 mL ethanol. For the 2nd feed solution, MMA, BA, and AA monomers are mixed according to their weight fraction in a beaker. The volumes of both the feed solutions are made up to 50 mL by adding ethanol. The two feed solutions are added dropwise into the refluxed solution, and the polymerization is run for about 2 hours at 90°C. At the end of the polymerization, the temperature is maintained at 90°C to partially evaporate the ethyl acetate, while 50–100 mL ethanol is continuously added to prevent the polymer from drying out.

Next, the solvent is displaced by adding water dropwise at 70°C inducing a macromolecular rearrangement of the polymer to form colloidally stable nanoparticles. The nanoparticulate suspension is continuously heated at 70°C to evaporate the remaining ethanol. Lastly, the nanoparticulate suspension is dialyzed for 24 hours to remove excess monomers and solvents. A wide range of nanoparticle sizes are obtained by varying the amount of ethanol added after the polymerization step. The size and zeta potential of the nanoparticles is measured by dynamic light scattering using Zetasizer Nano-ZS (Malvern, UK). In this work, nanoparticulate suspension (4%, w/v) of PMMA-MeOPEGMA nanoparticles having a mean diameter of 50 ± 20 nm and zeta potential of +30 mV are used in the spray-drying experiment. The PLGA nanoparticulate suspension (0.2%, w/v) are prepared by the nanoprecipitation method of[17] using acetonitrile as the solvent to produce 220 ± 50 nm nanoparticles. The pH of the nanoparticulate suspension is varied by adding hydrochloric acid or potassium hydroxide.

Spray-drying experiment

Büchi B-290 Mini Spray Dryer (Switzerland), which operates on the principal of a two-fluid atomizer, is employed in the experiment. The nozzle diameter used is 1.5 mm. The adjustable parameters in the experiments are the inlet temperature, the drying gas flow rate, and the feed flow rate. The following spray-drying condition is employed: inlet temperature of 110°C, atomizing gas flow rate of 250 L/h, and feed rate of 4.0 mL/min. The spray drier outlet temperature varies between 65°C and 70°C, which is slightly above the glass transition temperature of the PMMA-MeOPEGMA polymer (T_g = 65°C) determined by a differential scanning calorimetry (Perkin-Elmer, Waltham, MA, USA). The calculated drying time (τ_D) of a single 50-μm droplet at 100°C is ≈0.15 second, whereas the diffusion coefficient of 100 nm nanoparticles (D_S) is $\approx 10^{-12}$ m^2/s resulting in *Pe* of ≈1000 [Equation (1)]. Hence, the fast convective drying rate required to form the hollow nanoparticulate aggregates is satisfied at the current operating condition. After spray drying, the dry powders are dispersed in ultrapure water by a gentle mixing to create an injectable form of the hollow nanoparticulate aggregates.

Particle characterization

The hollow nanoparticulate aggregates are characterized in terms of their size, size distribution, shape, and shell thickness. The spray-dried particles are stored in a desiccator for a 48-hour-period before the characterization. The particle geometric diameter (d_G) is determined by light diffraction using Particle Size Analyzer MS2000 (Malvern, UK). The results reported are based on measurements of three aliquots with a minimum of 1000 sample counts each. The measurement uncertainty for the d_G measurement is approximately 5%. The particle shape information is obtained using a scanning electron microscope (SEM) model JSM-6700F JEOL (Peabody, MA, USA). Transmission electron microscope (TEM) model Tecnai-TF-20 FEI Company (Hillsboro, OR, USA) is used to examine the degree of hollowness of the particles. The samples for the image analysis are prepared by wetting the SEM carbon tape and TEM copper grid before sprinkling the particles onto them. The samples are dried in a desiccator before the analysis.

The ratio of the shell thickness to the particle radius [*S/R* ratio in Equation (2)] is quantified from the degree of hollowness characterized by the ratio of ρ_{eff}/ρ_{true}, where ρ_{eff} and ρ_{true} are the effective and true particle

densities, respectively. The derivation of Equation (2) is provided in the Appendix A. The effective particle density is defined as the particle mass divided by its total volume that includes the volume of the solid, hollow core, and pores, whereas the true particle density is calculated only based on its solid volume

$$\frac{S}{R}-1-\left(1-\frac{\rho_{\text{eff}}}{\rho_{\text{true}}}\right)^{1/3}. \tag{2}$$

The ratio of $\rho_{\text{eff}}/\rho_{\text{true}}$ is typically determined from direct measurements of the particle densities, where ρ_{true} and ρ_{eff} are determined by pycnometer (Ultrapcynometer1000) and tap densitometer (Autotap1000) of Quantachrome (Boynton Beach, FL, USA), respectively. The value of ρ_{eff} obtained from the tap densitometer, however, is not only influenced by the degree of hollowness of the particles but also by the interparticle surface forces. As a result, the tap density measurement is often inadequately sensitive to capture a small change in the degree of hollowness for particles with significant interparticle attractive forces (e.g., fine cohesive particles). In this work, the size of the hollow nanoparticulate aggregates must be less than 10 μm, hence significant interparticle forces are expected.

For that reason, this work proposes an alternative method to quantify ρ_{eff} to complement the tap density measurement. In inhaled drug delivery research, the particle geometric diameter (d_{G}) can be related to ρ_{eff} by the aerodynamic diameter (d_{A}) as described in Equation (3)[18] in which $\rho_{\text{S}} = 1$ g/cm^3. The aerodynamic diameter is defined as the diameter of a unit density spherical particle that settles through the air with a velocity equal to that of the particle in question. The d_{A} is typically used to characterize the distance traveled by the inhaled particle in the human respiratory airways and is measured in this work using the time-of-flight principle (PSDA 3603, TSI, USA). The results reported are based on three aliquots of 1000 sample counts each. The measurement uncertainty between the three replicates is less than 2%

$$\rho_{\text{eff}}-\rho_{\text{s}}\left(\frac{d_{\text{A}}}{d_{\text{G}}}\right)^2. \tag{3}$$

Taking into account the measurement uncertainties of both d_{G} and d_{A} (i.e., 5% and 2%, respectively), the uncertainty in the ratio of $\rho_{\text{eff}}/\rho_{\text{true}}$ calculated from Equation (3) is as follows:

$$\frac{\Delta\rho_{\text{eff}}}{\rho_{\text{eff}}}=2\left(\frac{\Delta d_{\text{G}}}{d_{\text{G}}}\right)+2\left(\frac{\Delta d_{\text{A}}}{d_{\text{A}}}\right)\approx 14\%. \tag{4}$$

Results and discussion

Shell thickness: Effect of the nanoparticulate suspension concentration

To obtain hollow nanoparticulate aggregates of varying shell thickness, we conduct the spray-drying experiment at a wide range of nanoparticle concentrations for both the PMMA-MeOPEGMA and the silica nanoparticles. The experimental results of the PMMA-MeOPEGMA and silica nanoparticles are summarized in Tables 1 and 2, respectively. At the current spray-drying operating condition, the experiments conducted using the PLGA and polystyrene nanoparticles fail to produce the hollow spherical nanoparticulate aggregates. Spray drying of the PLGA nanoparticles at a concentration of 0.5%

Table 1. Hollow nanoparticulate aggregates of PMMA-MeOPEGMA nanoparticles (50 ± 20 nm).

Run no.	NP conc. (% w/w)	Mean d_{G} (μm)	Median d_{G} (μm)	Mode d_{G} (μm)	d_{A} (μm)	$\rho_{\text{eff}}/\rho_{\text{true}}$	S/R_{theory} (%)	S_{theory} (nm)
P1	0.9	10.0 ± 3.8	6.7	7.3	3.0 ± 0.2	0.07	2.4	120
P2	1.2	9.6 ± 3.4	6.0	7.3	2.5 ± 0.1	0.05	1.8	90
P3	2.4	8.0 ± 3.3	5.5	4.6	3.1 ± 0.2	0.12	4.0	160
P4	3.2	9.1 ± 3.7	5.4	6.3	2.6 ± 0.1	0.06	2.1	100

Table 2. Hollow nanoparticulate aggregates of silica nanoparticles (20 ± 10 nm).

Run no.	NP conc. (% w/w)	Mean d_{G} (μm)	Median d_{G} (μm)	Mode d_{G} (μm)	d_{A} (μm)	$\rho_{\text{eff}}/\rho_{\text{true}}$	S/R_{theory} (%)	S_{theory} (nm)
S1	0.2	7.4 ± 3.6	2.4	2.3	2.6 ± 0.1	0.05	1.8	70
S2	0.3	4.9 ± 3.3	2.3	2.3	2.5 ± 0.1	0.11	3.9	100
S3	0.4	4.6 ± 2.9	2.4	2.0	2.4 ± 0.1	0.12	4.1	100
S4	0.7	5.4 ± 2.8	2.5	2.3	2.6 ± 0.1	0.10	3.5	100
S5	1.2	4.3 ± 3.9	2.3	2.3	2.3 ± 0.1	0.12	4.3	100

(w/w) results in the production of a mixture of dimpled spherical particles and irregular-shape particles (≈4–5 μm in length) that are not hollow (Figure 3A). The glass transition temperature of the PLGA is approximately 37°C[19], which is significantly below the spray dryer outlet temperature (i.e., 65–70°C). Consequently, the PLGA nanoparticles undergo an extensive deformation and softening attributed to the gained molecular mobility at a temperature above its T_g resulting in the formation of the irregular-shape particles.

The deformation of the PLGA nanoparticles can be minimized by lowering the spray dryer inlet temperature from 110°C to approximately 70°C, which indicates the need to use organic solvents, instead of ultrapure water, as the dispersion medium. This approach is not pursued in this work as our spray drier is not equipped to handle flammable solvents. On a similar note, spray drying of the polystyrene nanoparticles at a concentration of 0.2% (w/w) yields fine elliptical-shape nanoparticulate aggregates in (≈2 μm in length) that are not hollow (Figure 3B). The spray-drying experiments are repeated at concentrations of 0.4% and 1.0% (w/w) yielding similar results, which suggests that the current spray-drying operating condition is not suitable to produce hollow spherical aggregates of the polystyrene nanoparticles. The results of the PLGA and polystyrene nanoparticles signify the fact that in addition to satisfying the fast convective drying rate, all aspects of the spray-drying operation must be meticulously tuned to produce the hollow spherical particle morphology.

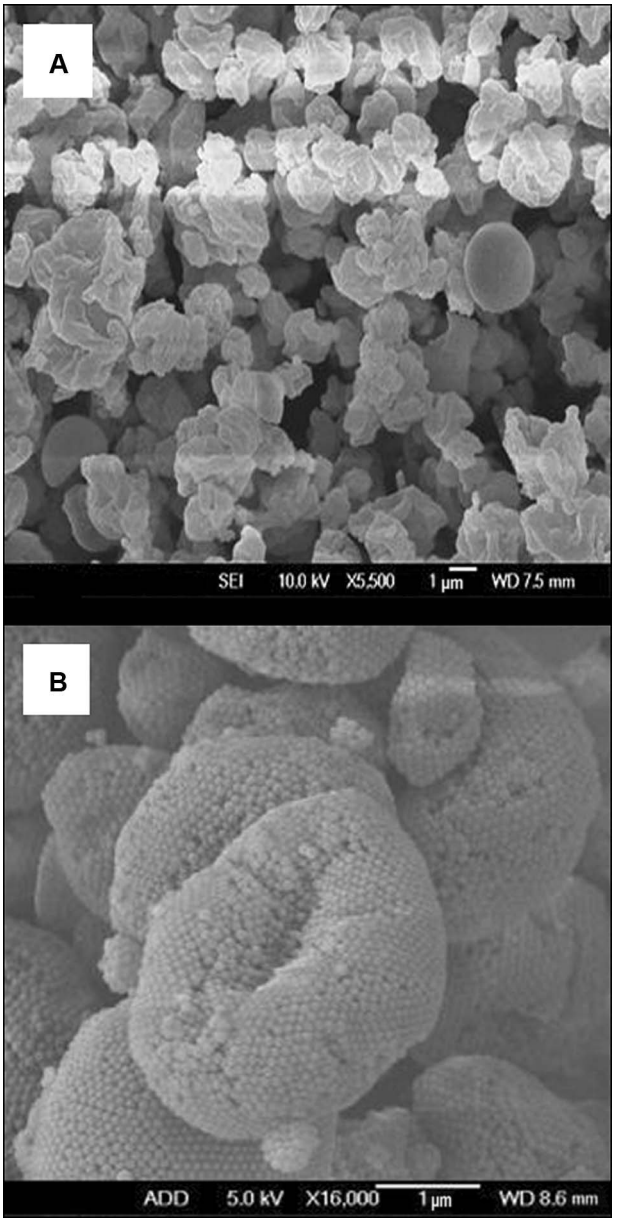

Figure 3. SEM images of (A) spray-dried PLGA nanoparticles at 0.5% (w/w) and (B) spray-dried polystyrene nanoparticles at 0.2% (w/w).

For the 50 ± 20 nm PMMA-MeOPEGMA nanoparticles (ρ_{true} = 1.3 g/cm^3), the spray-drying experiments are conducted at concentrations of 0.9%, 1.2%, 2.4%, and 3.2% (w/w). The spray-dried products, unlike the PLGA and polystyrene nanoparticles, are in the form of dimpled spherical aggregates with d_G between 5 and 10 μm (Figure 4A) similar to the findings of Hadinoto et al.[20] A closer look at one of the dimpled spheres with a defected shell reveals the hollow structure (Figure 4B). Importantly, a further increase in the nanoparticle concentration above 3.2% (w/w) results in the formation of fine nonhollow nanoparticulate aggregates, which is similar to the result of the polystyrene nanoparticles. Moreover, a close-up view at the particle surface in Figure 5A and B reveals that the shell constitutes of several layers of the nanoparticulate aggregates that form a gas-tight interface at the shell suited for use as an ultrasound contrast agent.

After being dispersed in ultrapure water, the suspension of the hollow nanoparticulate aggregates is ultrasonicated at a low intensity (40 kHz) for 5 minutes and centrifuged at 4300 × g at an ambient temperature. The resultant supernatant is analyzed using the Zetasizer to detect the presence of dispersed nanoparticles, if any. The Zetasizer analysis does not result in a significant change between the particle size distribution of the fresh ultrapure water, which is contributed by the inherent particulate impurities present in the water, and that of the supernatant. The result therefore indicates that nanoparticulate aggregates are not easily disintegrated into the primary nanoparticles in an aqueous environment, which are similar to the findings of Chaubal and Popescu[21], Chiou et al.[22], and Freitas and Muller[23] using nanoparticles of different chemical nature. A study to evaluate the shell structural stability under a high-intensity ultrasound excitation is currently ongoing and will be detailed in a forthcoming article.

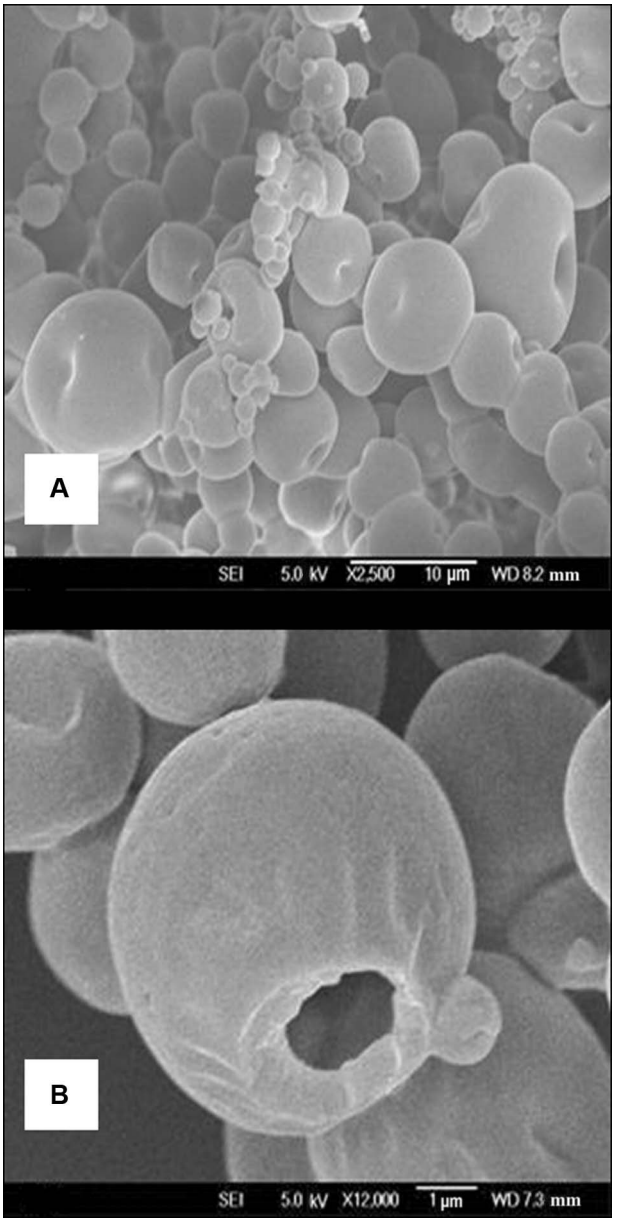

Figure 4. SEM images of the spray-dried PMMA-MeOPEGMA nanoparticles (A) dimpled sphere and (B) hollow structure (*Run No. P1*).

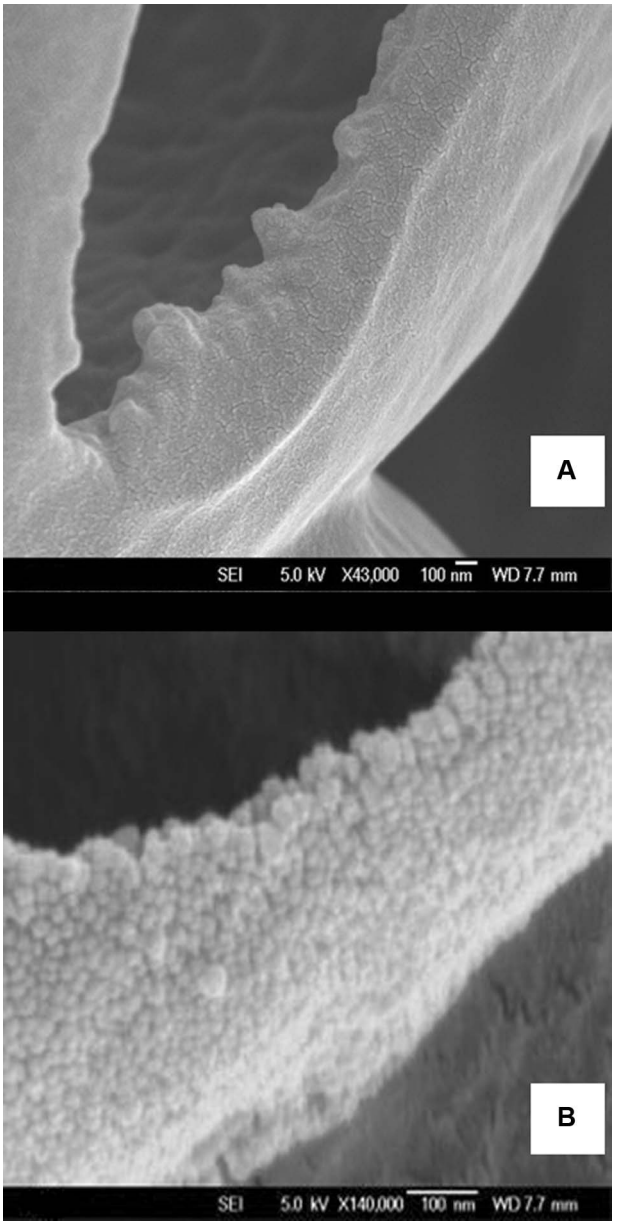

Figure 5. SEM images of the spray-dried PMMA-MeOPEGMA nanoparticles (A) a close-up view of the particle surface and (B) layers of the nanoparticulate aggregates constitute the shell (*Run No. P1*).

The results in Table 1 indicate that the mean geometric size and the particle size distribution are not greatly influenced by the change in the nanoparticle concentration. The mean d_G values vary between 8 and 10 µm for the range of nanoparticle concentration investigated. The median and mode d_G values denote that a majority of the particles are in the lower size range of 5–7 µm, hence the particles are smaller than the blood capillary size. The TEM images of the particles in Figure 6 indicate that all of these particles are hollow with varying shell thickness depending on their particle size, where the hollow structure is reflected in the noticeable difference between the contrasts of the shell and the core components. (Note: the cutoff TEM image shown in Figure 6F is caused by the limitation in the lowest magnification achievable in our TEM instrument, without switching to the 'Low Magnification Mode' that would jeopardize the image quality.)

The TEM images indicate that the small size particles ($d_G < 5$ µm) exhibit a higher S/R ratio ($S/R \approx 40\%$) compared with their larger size counterparts ($S/R \approx 20\%$). In the detailed analysis that follows, however, the TEM images are not to be utilized in quantifying the mean magnitude of the S/R ratio because 1) we find that using the TEM technique to obtain a representative sample

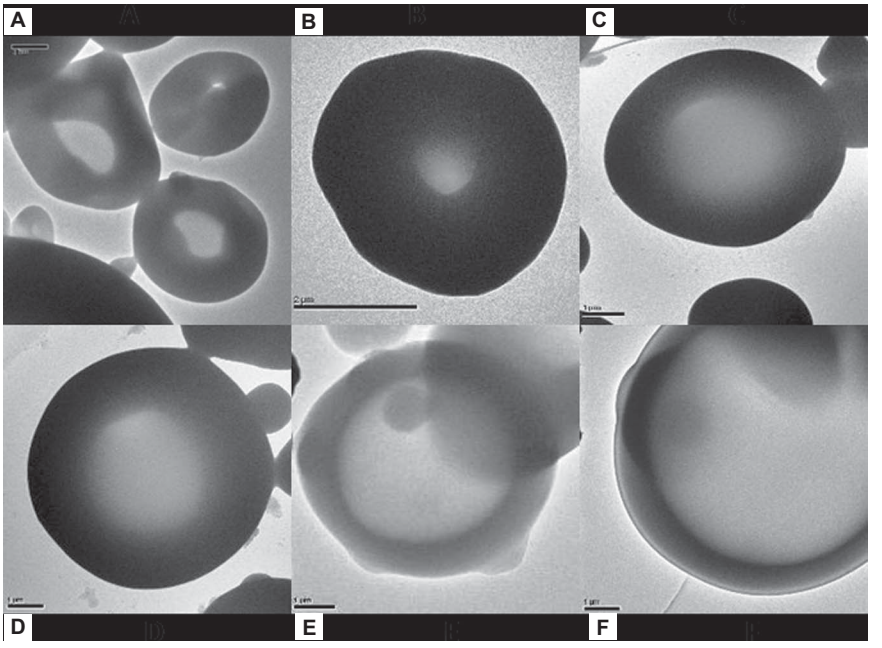

Figure 6. TEM images of the hollow microspheres with d_G equal to (A), 3 μm; (B), 4 μm; (C), 6 μm; (D), 7 μm; (E), 8 μm; and (F), 10 μm (*Run No. P1*).

size (>100) for this particle size range is implausible due to the excessive time required, and 2) the issues of overlapping images and a lack of sharp contrast between the shell and the core components, which are apparent in a majority of the TEM images presented in Figure 6, are predicted to result in less than accurate *S/R* ratio estimates. Therefore, the *S/R* ratio is quantified in this work using the ratio of ρ_{eff}/ρ_{true} outlined in the Section 2.4 and is validated by the SEM images.

Similar to the trend in d_G, the mean aerodynamic diameter does not significantly vary ($d_A \approx 2.5$–3 μm) with the change in the nanoparticle concentration (Table 1). As a result, the ratio of ρ_{eff}/ρ_{true} calculated from Equation (3) is relatively constant at 0.05–0.07. One exception is for the *Run No. P3* in which the ratio of ρ_{eff}/ρ_{true} is equal to 0.12. For comparison, the ratio of ρ_{eff}/ρ_{true} obtained from the tap density measurement yields a constant value of 0.09 for all of the runs, which reaffirms the inadequacy of the tap density method in detecting a small change in the degree of hollowness[24].

Next, the theoretical *S/R* ratio is calculated using Equation (2) to be equal to 4% for the *Run No. P3*, whereas it is equal to approximately 2% for the other three runs. Significantly, the difference between the two *S/R* ratio results is larger than the measurement uncertainty [i.e., 14% from Equation (4)]. Therefore, it can be construed that the hollow nanoparticulate aggregates with the lower mean d_G value (i.e., *Run No. P3*) exhibit a higher *S/R* ratio, which agrees with the observation from the TEM images. Despite this agreement, the magnitude of the theoretical *S/R* ratio (i.e., 2–4%) is one order of magnitude smaller than the experimental value obtained from the TEM images (i.e., 20–40%).

To examine which of the two estimated *S/R* ratios represents the actual value, we conduct SEM imaging of purposely fragmented particles to measure their shell thickness. The hollow nanoparticulate aggregates are ground in a mixer mill (Retsch Mill, Cole Palmer, CA, USA) for 15 minutes to obtain hollow particles with defected shells. Two of the SEM images from *Run No. P1* and *P4* are presented in Figures 7 and 8, respectively, which reveal that 10–15 layers of the aggregates of the 50 ± 20 nm nanoparticles constitute the shells. The geometric size of the hollow particle in Figure 7 (≈8 μm) is 1.6 times larger than that in Figure 8 (≈5 μm). The shell thickness values measured from the SEM images are 220 and 170 nm, which correspond to the *S/R* ratios of 5.5% and 6.8%, respectively. The largest shell thickness recorded from the many SEM images is 500 nm for a hollow particle of d_G = 25 μm, which corresponds to the *S/R* ratio of 4% (Figure 9).

Importantly, the measured values of the shell thickness from the SEM images are in relatively close agreement with the theoretical values estimated by Equation (2). Overall, the theoretical *S/R* ratios only differ by 3–4% points from the measurement using the SEM images. Hence, the method of estimating the *S/R* ratio from the ratio of ρ_{eff}/ρ_{true} has been validated and proven to be superior to the TEM analysis. In this work, the shortcoming of the TEM analysis is believed to be caused by an unavoidable occurrence of overlapping particles (see Figures 7A and 8A) during the sample preparation

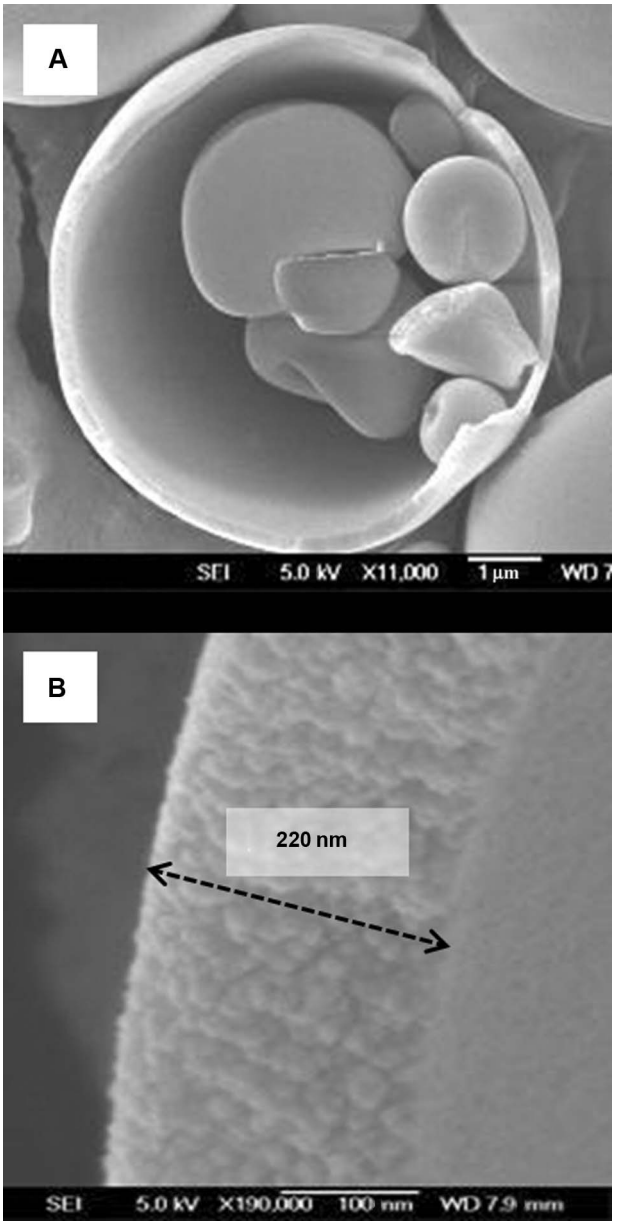

Figure 7. SEM images of the fragmented particle (A) 8 µm hollow microspheres and (B) shell thickness (*Run No. P1*).

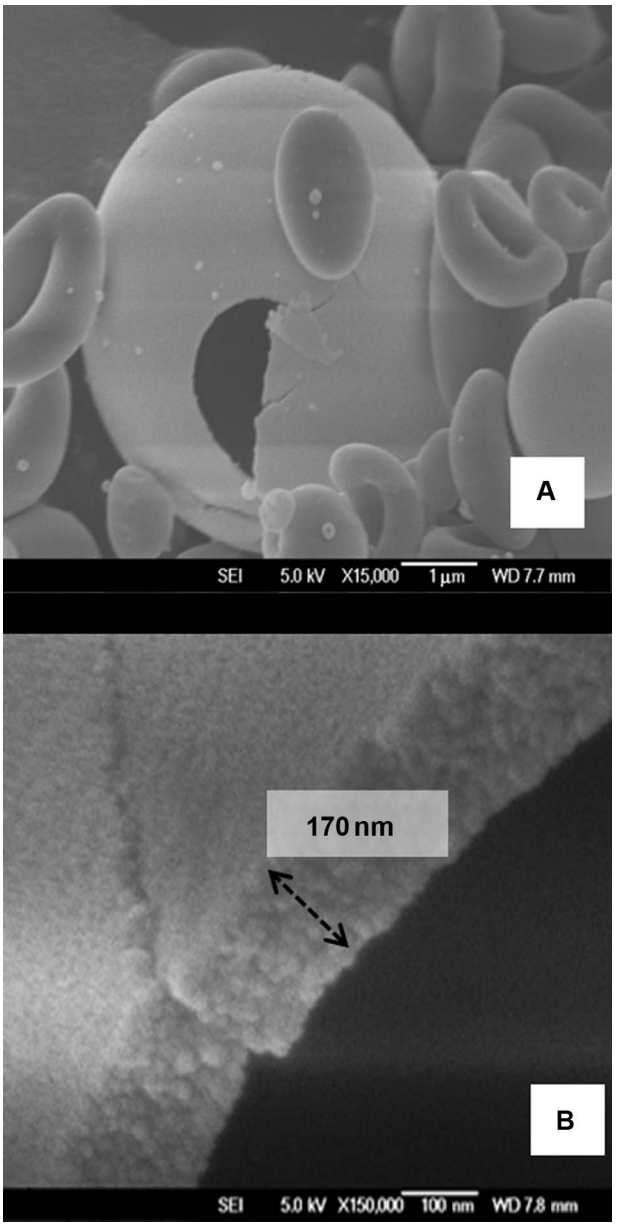

Figure 8. SEM images of the fragmented particle (A) 5 µm hollow microspheres and (B) shell thickness (*Run No. P4*).

process, which influences the contrast produced by the electron beam.

Next, the spray-drying experiments are conducted at the same operating condition using the 20 ± 10 nm silica nanoparticles (ρ_{true} = 2.3 g/cm^3) at nanoparticle concentrations between 0.2% and 1.2% (w/w). The mean d_G values in Table 2 indicate that the spray-dried particles of the silica nanoparticles are smaller than those of the PMMA-MeOPEGMA nanoparticles. The median and mode d_G values indicate that the lower mean d_G value is partly attributed to a large amount of very fine ($d_G \approx 2$ µm) hollow nanoparticulate aggregates being produced. The SEM image of the silica hollow nanoparticulate aggregates in Figure 10 reaffirms the abundant presence of the very fine particles similar to the result of Iskandar et al.[25] As the nanoparticle concentration is raised above 0.2% (w/w), the mean d_G decreases from ≈7 to 5 µm, whereas the mean d_A remains relatively constant at 2.5 µm. As a result, the theoretical *S/R* ratios are calculated to be between 2% and 4%, which are similar to the results of the PMMA-MeOPEGMA nanoparticles.

Importantly, the results also indicate that the hollow nanoparticulate aggregates with the lower mean d_G values (*Runs No. S2–S4*) exhibit the higher *S/R* ratios. Nevertheless, the results of both the polymer and the

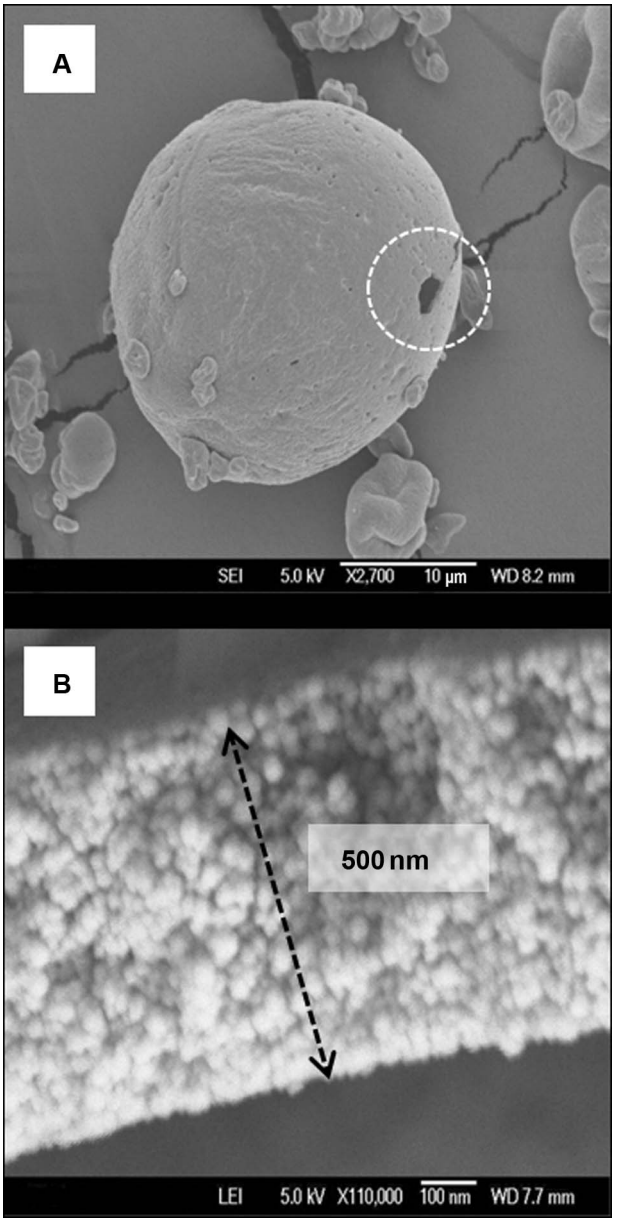

Figure 9. SEM images of the largest shell thickness recorded (A) 25 µm hollow microspheres and (B) shell thickness (*Run No. P1*).

silica nanoparticles suggest that increasing the nanoparticle concentration (i.e., ≈ up to fivefold) does not result in a significant change in the magnitude of the *S/R* ratio, which is only raised from 2% to 4%. Therefore, alternative approaches to modulate the *S/R* ratio are examined and detailed in the next section.

Shell thickness: Effects of the spray-drying operating condition and pH

First, the impact of changing two parameters that govern the spray-drying process is examined. The two parameters are 1) the inlet temperature, which influences the convective drying rate and 2) the ratio of the feed flow rate to the gas atomizing flow rate, which influences the sprayed droplet size. Second, the effect of the nanoparticulate suspension pH that influences the colloidal stability of the nanoparticles and their diffusivity[26] is examined. The experiments are conducted using the 20 ± 10 nm silica nanoparticles, which have been shown to exhibit a similar trend in their shell thickness variation with the 50 ± 20 nm PMMA-MeOPEGMA nanoparticles.

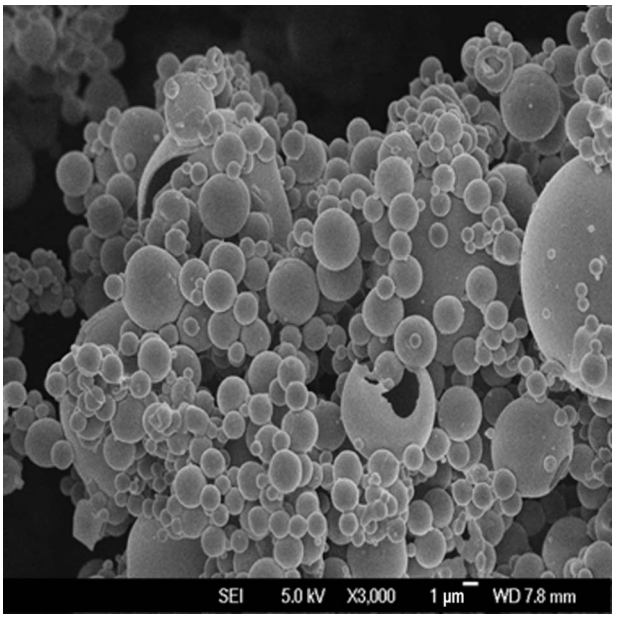

Figure 10. SEM image of the spray-dried silica nanoparticles (*Run No. S4*).

At 0.7% (w/w) nanoparticle concentration, the results in Table 3 (*Runs No. 1 and 2*) indicate that changing the two spray-drying parameters (i.e., the inlet temperature is raised from 110°C to 130°C, the feed to gas ratio is reduced by 40%) does lead to a change in the mean d_G of the hollow nanoparticulate aggregates. However, the *S/R* ratios are not greatly affected by the change in the particle size and remain in the 4% range. Significantly, the results presented in Tables 2 and 3 indicate that the magnitude of the *S/R* ratios obtained at the current operating condition and its vicinity are relatively similar despite the changes introduced in the experimental condition. For that reason, the feasibility of producing hollow nanoparticulate aggregates with considerably larger *S/R* ratios is explored by running the spray-drying experiment in a distant operating region, such as at a different pH and at a completely different spray-drying operating condition (i.e., inlet temperature at 120–140°C, feed flow rate of 1.7–5.8 mL/min, and gas flow rate of 320–420 L/h).

In that regard, reducing the pH of the nanoparticulate suspension from 7 to 5 (*Runs No. 3 and 4*) leads to

Table 3. Effects of spray drying operating condition and pH on the shell thickness.

Run no.	NP conc. (% w/w)	pH	T (°C)	Feed rate (mL/min)	Air flow (L/h)	Morphology	Mean d_G	ρ_{eff}/ρ_{true}	S/R (%)
S4	0.7	7	110	4.0	250	hollow microspheres	5.4	0.10	3.5
1	0.7	7	130	4.0	250	hollow microspheres	6.2	0.13	4.5
2	0.7	7	110	4.0	360	hollow microspheres	4.9	0.12	4.2
3	0.7	5	120	5.8	420	fine microspheres	2.8	0.17	6.0
4	0.7	5	140	1.7	420	fine microspheres	1.9	0.21	7.5
5	0.7	9	120	1.7	420	crumpled particles	2.9	0.17	NA[a]
6	0.7	9	120	5.3	360	crumpled particles	3.8	0.16	NA[a]
7	0.7	9	140	5.8	420	crumpled particles	4.3	0.16	NA[a]
8	0.7	9	140	1.7	320	crumpled particles	5.7	0.17	NA[a]

[a]the shape is no longer a hollow core-shell structure.

the production of fine hollow spherical nanoparticulate aggregates ($d_G \approx 2$–3 μm). The increased production of the fine particles at pH = 5 is independent of the spray-drying parameters selected. Importantly, the *S/R* ratio is now almost doubled to 6–8% range, which is not unexpected as the previous results at pH = 7 have shown that the smaller-size particles exhibit a higher *S/R* ratio. The doubled *S/R* ratio, however, is negated with the substantial reduction in the particle size that may negatively affect the particle echogenicity level, which is as important as the shell stability if these particles are to be used as an ultrasound contrast agent.

In contrast, raising the pH to 9 leads to the production of crumpled particles though with an apparent increase in their shell thickness (see Figure 11 inset). Importantly, the crumpled particles are consistently produced at pH = 9 and unaffected by the spray-drying parameters selected (*Runs No. 5–8*). Unfortunately, the crumpled shape makes the gas no longer encapsulated within the shell, which renders the particles not suitable for use as an ultrasound contrast agent. The crumpled shape is thought to be caused by an excessive buckling of the original shell during the drying process[27], which is caused by the change in the magnitude of the interparticle interaction forces in the drying droplet when the pH is modified.

The significant impact of the pH on the *S/R* ratio and the minimal impact of the spray-drying operating condition on the ratio signify the fact that, instead of modifying the macroscopic drying process, the *S/R* ratio may be better controlled by modifying the parameters acting at the nanoparticle scale (e.g., pH, nanoparticle size, nanoparticle surface charge, and surfactant inclusion).

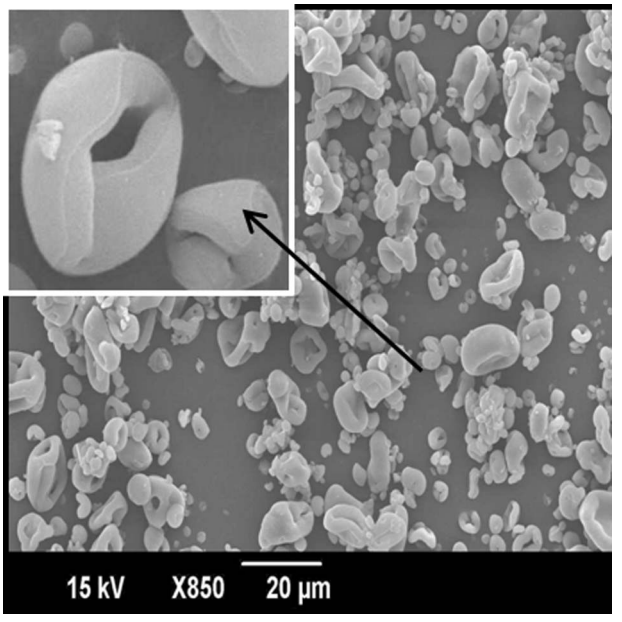

Figure 11. SEM image of the crumpled particles (inset: larger shell thickness).

In that regard, preliminary results on the spray-drying experiments using nanoparticles of a larger size (i.e., 170 ± 80 nm PMMA-MeOPEGMA nanoparticles) are presented in Table 4. Using a larger nanoparticle size, hollow nanoparticulate aggregates having significantly higher *S/R* ratios (i.e., up to 16%) can be produced without significantly reducing the particle mean size. For that reason, a detailed study on the effects of the nanoparticle size and surfactant inclusion on the *S/R* ratio is being carried out in our laboratory.

Table 4. Hollow nanoparticulate aggregates of PMMA-MeOPEGMA nanoparticles (170 ± 80 nm).

Run no.	NP conc. (% w/w)	Mean d_G (μm)	Median d_G (μm)	Mode d_G (μm)	d_A (μm)	ρ_{eff}/ρ_{true}	S/R_{theory} (%)	S_{theory} (nm)
P5	1.0	4.2 ± 3.3	3.0	3.7	2.7 ± 0.1	0.32	12	250
P6	1.5	4.0 ± 2.7	2.0	3.0	2.9 ± 0.1	0.41	16	320

Conclusion

A novel spray-drying technique to manufacture hollow spherical nanoparticulate aggregates that can potentially be employed as an ultrasound contrast agent is presented. The principle mechanism is based on a fast convective drying of sprayed droplets containing nanoparticles resulting in the formation of hollow core-shell structures of the nanoparticulate aggregates. Silica and polymeric nanoparticles (diameter <100 nm) are used as the model nanoparticles. The mean geometric size of the spray-dried hollow nanoparticulate aggregates varies between 2 and 10 μm, hence they are suitable for use as an ultrasound contrast agent in tissue perfusion imaging. A preliminary study on the shell structural stability reveals that the nanoparticulate aggregates suspended in water are not easily disintegrated under ultrasonication.

The magnitude of the shell thickness-to-particle radius (*S/R*) ratio obtained from a wide range of experimental conditions remains relatively constant at 2–4% for both the polymer and the silica nanoparticles. The smaller-size particles consistently exhibit a higher *S/R* ratio than their larger size counterparts hence signifying higher shell stability. Specifically, the *S/R* ratio is not significantly affected by the changes in the spray-drying nanoparticle concentration and operating condition (e.g., inlet temperature, feed rate, and drying gas rate), as long as a fast convective drying rate is satisfied and a maximum threshold in the nanoparticle concentration is not surpassed. On the contrary, changing the pH of the nanoparticulate suspension significantly influences the spray-dried particle morphology and consequently the *S/R* ratio. In addition, the experiment conducted using a larger nanoparticle size (diameter ≈200 nm) results in a substantial increase in the *S/R* ratio (≈12–16%). The results of the pH and the nanoparticle size effects suggest that the *S/R* ratio can be modulated more easily by modifying the process parameters acting at the nanoparticle scale (e.g., nanoparticle size, surface forces) rather than modifying the macroscopic drying process at the micron-size droplet scale.

Acknowledgments

A financial support from Nanyang Technological University's Start-Up Grant (Grant No. SUG 8/07) is gratefully acknowledged. The authors thank Selina Li for her contribution in the spray-drying experiment.

Declaration of interest: The authors report no conflicts of interest.

References

1. Klibanov AL. (1999). Targeted delivery of gas-filled microspheres, contrast agents for ultrasound imaging. Adv Drug Deliv Rev, 37(1–3):139–57.
2. Lindner JR. (2004). Microbubbles in medical imaging: Current applications and future directions. Nat Rev Drug Discov, 3(6):527–32.
3. Klibanov AL. (2002). Ultrasound contrast agents: Development of the field and current status, Contrast Agents Ii. Top Curr Chem, 222:73–106.
4. Ferrara K, Pollard R, Borden M. (2007). Ultrasound microbubble contrast agents: Fundamentals and application to gene and drug delivery. Ann Rev Biomed Eng, 9:415–47.
5. Krasovitski B, Kimmel E. (2006). Stability of an encapsulated bubble shell. Ultrasonics, 44(2):216–20.
6. Landau LD, Lifshitz EM. (1976). Mechanics, 1. New York: Pergamon Press.
7. Raisinghani A, DeMaria AN. (2001). Physical principles of microbubble ultrasound contrast agents, Symposium on Contrast Echocardiography (CE), Newport, Rhode Island, 3J–7J.
8. Bjerknes K, Sontum PC, Smistad G, Agerkvist I. (1997). Preparation of polymeric microbubbles: Formulation studies and product characterisation. Int J Pharm, 158(2):129–36.
9. El-Sherif DM, Wheatley MA. (2003). Development of a novel method for synthesis of a polymeric ultrasound contrast agent. J Biomed Mater Res Part A, 66A(2):347–55.
10. Narayan P, Wheatley MA. (1999). Preparation and characterization of hollow microcapsules for use as ultrasound contrast agents. Polymer Eng Sci, 39(11):2242–55.
11. Straub JA, Chickering DE, Church CC, Shah B, Hanlon T, Bernstein H. (2005). Porous PLGA microparticles: AI-700, an intravenously administered ultrasound contrast agent for use in echocardiography. J Control Release, 108(1):21–32.
12. Pisani E, et al. (2006). Polymeric nano/microcapsules of liquid perfluorocarbons for ultrasonic imaging: Physical characterization. Langmuir, 22(9):4397–402.
13. Schmidt W, Roessling G. (2006). Novel manufacturing process of hollow polymer microspheres. Chem Eng Sci, 61(15):4973–81.
14. Hadinoto K, Zhu K, Tan RBH. (2007b). Drug release study of large hollow nanoparticulate aggregates carrier particles for pulmonary delivery. Int J Pharm, 341(1–2):195–206.
15. Rossi S, Waton G, Krafft MP. (2008). Small phospholipid-coated gas bubbles can last longer than larger ones. Chemphyschem, 9(14):1982–5.
16. Tsapis N, et al. (2005). Onset of buckling in drying droplets of colloidal suspensions. Phys Rev Letters, 94(1):018302(1–4).
17. Govender T, Stolnik S, Garnett MC, Illum L, Davis SS. (1999). PLGA nanoparticles prepared by nanoprecipitation: Drug loading and release studies of a water soluble drug. J Control Release, 57(2):171–85.
18. Edwards DA, Dunbar C. (2002). Bioengineering of therapeutic aerosols. Ann Rev Biomed Eng, 4:93–107.
19. Park PIP, Jonnalagadda S. (2006). Predictors of glass transition in the biodegradable polylactide and poly-lactide-co-glycolide polymers. J Appl Polymer Sci, 100(3):1983–7.
20. Hadinoto K, Phanapavudhikul P, Kewu Z, Tan RBH. (2007a). Dry powder aerosol delivery of large hollow nanoparticulate aggregates as prospective carriers of nanoparticulate drugs: Effects of phospholipids. Int J Pharm, 333(1–2):187–98.
21. Chaubal MV, Popescu C. (2008). Conversion of nanosuspensions into dry powders by spray drying: A case study. Pharma Res, 25(10):2302–8.
22. Chiou H, Chan HK, Heng D, Prud'homme RK, Raper JA. (2008). A novel production method for inhalable cyclosporine A powders by confined liquid impinging jet precipitation. J Aero Sci, 39(6):500–9.
23. Freitas C, Muller RH. (1998). Spray-drying of solid lipid nanoparticles SLN (TM). Eur J Pharm Biopharm, 46(2):145–51.
24. Abdullah EC, Geldart D. (1999). The use of bulk density measurements as flowability indicators. Powder Technology, 102(2):151–65.
25. Iskandar F, Gradon L, Okuyama, K. (2003). Control of the morphology of nanostructured particles prepared by the spray drying of a nanoparticle sol. J Coll Inter Sci, 265(2):296–303.

26. Bergna H, Roberts WO. (2006). Colloidal Silica, FL: CRC Press Taylor & Francis.
27. Sugiyama Y, Larsen RJ, Kim JW, Weitz DA. (2006). Buckling and crumpling of drying droplets of colloid-polymer suspensions. Langmuir, 22(14):6024–30.

Appendix A: Derivation of shell thickness-to-radius ratio (*S/R*)

For a hollow sphere (Figure A1) with a shell thickness S and a radius R, the ratio of S/R can be related to the true and effective particle densities by the following:

$$\rho_{\text{eff}} = \frac{m_{\text{shell}}}{V_{\text{shell}} + V_{\text{core}}}$$

$$\rho_{\text{true}} = \frac{m_{\text{shell}}}{V_{\text{shell}}}$$

$$\frac{\rho_{\text{eff}}}{\rho_{\text{true}}} = \frac{V_{\text{shell}}}{V_{\text{shell}} + V_{\text{core}}} = \frac{4/3\pi R^3 - 4/3\pi (R-S)^3}{4/3\pi R^3} 1 - \left(\frac{R-S}{R}\right)^3$$

$$\frac{R-S}{R} = \left(1 - \frac{\rho_{\text{eff}}}{\rho_{\text{true}}}\right)^{1/3}$$

$$\frac{S}{R} = \left(1 - \frac{\rho_{\text{eff}}}{\rho_{\text{true}}}\right)^{1/3}$$

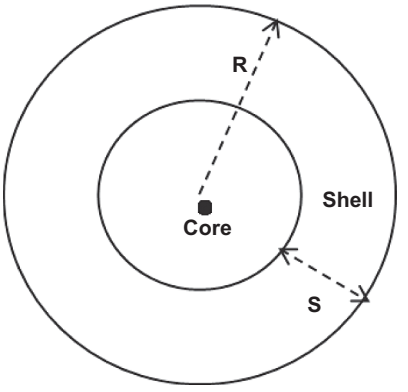

Figure A1. Shell thickness to particle radius ratio.